

Boron Nitride Nanotubes for Heat Dissipation in Polycaprolactone Composites

Thomas Pietri, Benjamin J. Wiley, and Jean-Pierre Simonato*

Cite This: *ACS Appl. Nano Mater.* 2021, 4, 4774–4780

Read Online

ACCESS |



Metrics & More



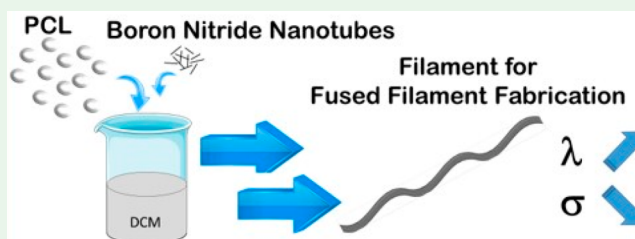
Article Recommendations



Supporting Information

ABSTRACT: This article describes the synthesis of nanocomposites for the fabrication of printable filaments of interest for additive manufacturing. Boron nitride nanotubes (BNNTs) stand out from several nanofillers for the improvement of heat dissipation from polycaprolactone (PCL) nanocomposites. At 30 wt % BNNT content, a 4-fold increase of the heat conductivity was measured compared to pristine PCL. However, such loadings alter the rheological properties in the molten state, rendering the nanocomposite unprocessable by fused filament fabrication (FFF) printers. At lower loading (i.e., 10 wt %), a trade-off was achieved, allowing improved heat dissipation performance and easy processability. This was exemplified through a 3D printed radiator as a proof of concept. The approach described herein could enable the development of high performance heat dissipation filaments for FFF fabrication processes.

KEYWORDS: boron nitride nanotubes, nanocomposites, thermal conductivity, viscosity, 3D printing, fused filament fabrication



1. INTRODUCTION

Additive manufacturing has become a powerful tool to fabricate objects on-demand with specific architectures and chemical compositions. It is seen as a highly flexible technology with potential in various fields such as healthcare,¹ batteries,² automotive,³ and aerospace,⁴ to name but a few. Many different families of materials can be processed, often at different scales by additive manufacturing, including ceramics,⁵ metals,⁶ cements,⁷ biomaterials,⁸ and so forth. One of the most widespread additive manufacturing technologies is fused deposition modeling, also known as fused filament fabrication (FFF). It is based on the use of thermoplastic-based filaments, which are heated to their melting points and then extruded, layer by layer, joining layers of materials to build a 3D object from a surface.⁹ Most of the materials currently in use are made of pristine thermoplastics or composites. Although the development of new materials with improved properties is an active field of research, only a rather moderate number of filaments with specific properties are commercially available.^{9–11} From an application point of view, high performance materials for electrical and thermal conduction (or insulation) are still needed. Significant progress has been achieved for the fabrication of conductive printable filaments, in particular by the use of metallic nanowires as fillers.^{12,13} Concerning thermal conduction, nanocomposites have shown improved properties but very few of them have been developed for additive manufacturing.^{14–16} This can be ascribed to the fact that the filament material not only be the desired thermal characteristics but also be printable. Applications for such filament materials include thermal management in plastic substrates for

electronic devices or in plastic battery casings.^{17–19} In these cases, the interest in additive manufacturing is growing steadily, in particular for the fabrication of on-demand specific shapes. The use of heat sinks has become essential for such applications in protecting the active components or systems from failure. In particular, enhanced heat dissipation is desirable in areas close to electrically active devices, such as batteries or electronics. In such cases, utilization of a heat sink with electrically insulating properties can prevent undesired effects originating from uncontrolled dispersion of charges such as short-circuit current or electrostatic discharge. The possibility to deposit heat sink or/and to fabricate radiators on localized spots, possibly on complex 3D-shaped surfaces, is a challenge for which 3D printing appears promising. To achieve this goal, there is a market need to reach high thermal conductivity coupled with electrically insulation, with easily processable filaments. In this report, we show that the properties of a simple and low-cost matrix made of polycaprolactone (PCL) can be significantly improved by the loading of nanofillers. PCL was used as the polymer matrix because it offers significant advantages such as a low melting point (57–65 °C) which gives access to a low printing temperature, a good resistance to water and lipophilic

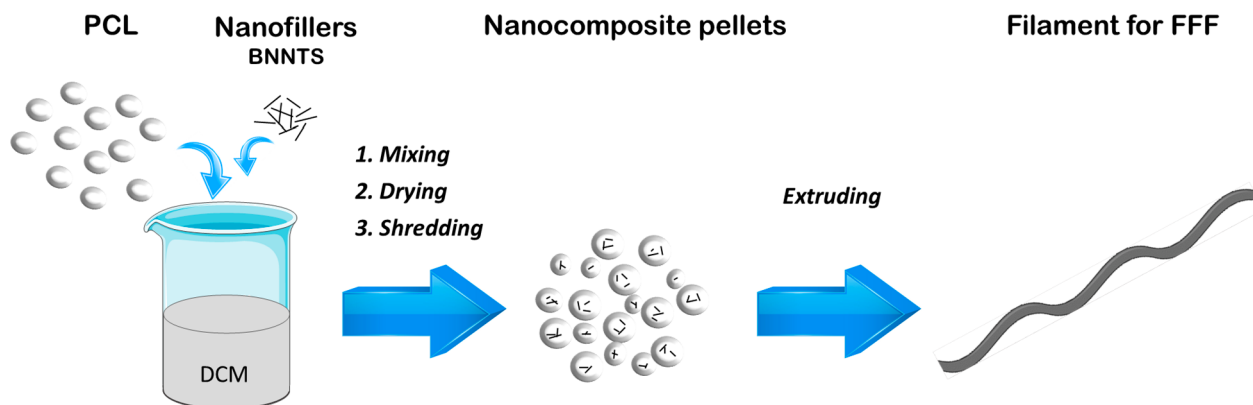
Received: February 4, 2021

Accepted: March 22, 2021

Published: April 16, 2021



Scheme 1. Fabrication Process for the Nanocomposites



chemicals, and a long-term mechanical stability.²¹ It is also a biodegradable polyester, and it is not prone to warping effects under adequate processing parameters. So as to limit the number of variables during this study, only one molecular weight ($M_n = 80\,000\text{ g}\cdot\text{mol}^{-1}$) of the polymer was used. Another reason for choosing PCL relies on its ability to dissolve steadily in dichloromethane (DCM), allowing a straightforward process for the fabrication of the nanocomposites.

The main point of this study is the demonstration that through fine choice of nanofillers it is possible to improve the thermal conductivity of the composite while keeping the electrical conductivity at a very low level. We show that beyond the chemical nature of the nanofillers, the form factor plays a crucial role as shown by the use of allotropes of hexagonal boron nitride nanoparticles with 1D and 2D dimensionalities. In addition, we also demonstrate that the intrinsic thermal properties of the nanocomposites are not the only point to be taken into consideration when selecting a material for 3D printing fabrication because the viscosity is drastically modified with the incorporation of the nanofillers. Thus, an optimal trade-off should be determined between the thermal properties and the processability. To our knowledge, this is the first study dealing with the use of boron nitride nanotubes (BNNTs) as nanofillers for the fabrication of 3D processable nanocomposites. The results appear very appealing for the development of new materials printable by the FFF technology, with both enhanced thermal conductivity and electrical insulating properties.

2. EXPERIMENTAL SECTION

2.1. Materials. PCL $M_w \sim 80\,000\text{ g}\cdot\text{mol}^{-1}$ and dichloromethane were purchased from Aldrich. AlN (purity 99.5%, 65–75 nm), SiC (purity 99%, 40–60 nm), and h-BN (purity 99.8%, 70–80 nm) were purchased from US Research Nano. BNNTs were purchased from BNNano as Nanobarbs (purity 90%, diameter 60 nm/length 20 μm).

2.2. Fabrication of Filaments and Printing Parameters. Filaments were fabricated by a Filament Maker Precision Series from 3DEVO, which consists of a single screw extruder with four temperature controllers and two pullers regulated by an optical detector. The optimized parameters for pure PCL and the 10 wt % BNNT nanocomposite were the following: temperature screw profile from feeder to nozzle of 65 °C–95 °C–95 °C–88 °C, speed screw rotation of 2.5 rpm, and filament diameter requirement of $1.75 \pm 0.10\text{ mm}$.

Preliminary printing experiments were performed on a Prusa MK3 printer (Prusa Research), and the radiators were 3D printed using a 3D-FFF HYDRA 430 from HYREL 3D. The optimized parameters

for pristine PCL were the following: substrate at 25 °C, 0.5 mm printing nozzle at 140 °C, printing speed of $15\text{ mm}\cdot\text{s}^{-1}$, and layer height of 0.25 mm. A poly(ether imide) (PEI) substrate was used to avoid warping. The optimized parameters for the 10 wt % BNNT nanocomposite were the following: substrate at 25 °C, 0.8 mm printing nozzle at 250 °C, printing speed of $15\text{ mm}\cdot\text{s}^{-1}$, and layer height of 0.4 mm.

2.3. Characterizations. Density was measured in a 1 cm^3 cell with a He gas displacement pycnometry system Accupyc II 1340 from Micromeritics, and the average value was calculated from 50 measurements. Specific heat capacity was obtained by a C80 Calvet calorimeter from Setaram Instrumentation. Two measurements were carried out for each material. After a 60 min plateau at 20 °C, the ramp-up temperature was set to $0.1\text{ }^\circ\text{C}\cdot\text{min}^{-1}$ up to 60 °C, and the sample was then maintained at 60 °C for 60 min. Electron microscopy images were obtained from a LEO 1530 scanning electron microscope from Zeiss. Thermal diffusivity was measured using a LFA 447 Nanoflash from Netzsch. The measurements were performed on disks (12.7 mm diameter, 1.5 mm thickness) obtained by a hydraulic press with heating plates. Each material was analyzed with three different samples, each measured five times. Thermogravimetric analysis (TGA) was performed on a TG92 analyzer from Setaram Instrumentation. Two measurements were carried out for each material. A heating rate of 5 °C/min up to 600 °C was applied under air atmosphere. Differential scanning calorimetry (DSC) measurements were completed using a LFA 401 apparatus from Netzsch, at a heating rate of 5 °C/min and cooling rate of 15 °C/min under He atmosphere. First, the sample was heated from –90 to 100 °C and was held for 5 min to remove thermal history of the sample. Second, a ramp from 100 °C to –90 °C with a 5 min plateau was realized. Finally, a second ramp-up was performed from –90 to 100 °C to obtain the melting curve. Glass temperature (T_g) and melting temperature (T_m) were extracted from the second ramp-up curve, and the crystallinity of the sample was calculated according to eq 1:

$$\chi = \frac{\Delta H_m}{\Delta H_m^\infty} \times 100 \quad (1)$$

where χ is the polymer crystallinity (%), ΔH_m is the melting enthalpy of the sample (J/g), and ΔH_m^∞ is the melting enthalpy of pure single crystal of PCL (J/g) selected as $135\text{ J}\cdot\text{g}^{-1}$.²⁰ Rheological measurements were performed with a Bohlin Gemini 2 from Malvern Instruments in oscillation mode with a parallel plate configuration (plate diameter = 20 mm). Samples (discs of 25 mm diameter and 1 mm thickness) were molded with a hydraulic press with heating plates directly from pellets. Sheet resistances (R_s) were measured at room temperature with a Hiستا-UX MCP-HT800 resistivimeter.

3. RESULTS AND DISCUSSION

The first step of this study was focused on benchmarking various electrically insulating nanomaterials, all selected for their high thermal conductivity. The chosen nanoparticles were

silicon carbide (SiC), aluminum nitride (AlN), and hexagonal boron nitride (h-BN), the latter being also introduced in the form of nanotubes (BNNTs). Although it is possible to extract some values from the literature for these nanomaterials, a significant discrepancy of the thermal properties figures was detected. Thus, we first chose to measure their densities and specific heat capacities with the same analytical systems under identical protocols. These data are presented in Table S1.

3.1. Fabrication of Nanocomposites. The nanocomposites were prepared according to the process presented in Scheme 1. After dissolution of the PCL in DCM, the nanomaterials were dispersed under vigorous agitation. After evaporation of DCM, the matrix was passed through a shredder and the resulting pellets were used for the fabrication of filaments and further characterization.

3.2. Characterization of the Nanocomposites. The thermal conductivity of the nanocomposites can be obtained through a set of measurements. Indeed the thermal conductivity can be calculated according to eq 2:

$$\lambda = \alpha \times \rho \times C_p \quad (2)$$

where λ is the thermal conductivity ($\text{W}\cdot\text{m}^{-1}\cdot\text{K}^{-1}$), α is the thermal diffusivity ($\text{m}^2\cdot\text{s}^{-1}$), ρ the density ($\text{kg}\cdot\text{m}^{-3}$), and C_p the specific heat capacity ($\text{J}\cdot\text{kg}^{-1}\cdot\text{K}^{-1}$).

First, the intrinsic thermal conductivity of PCL was measured at $0.19 \text{ W}\cdot\text{m}^{-1}\cdot\text{K}^{-1}$ which is perfectly consistent with reported values.^{22,23} The thermal conductivity values of the nanocomposites were measured at various loadings from 0 to 30 wt %. The results are plotted in Figure 1. Filler loadings

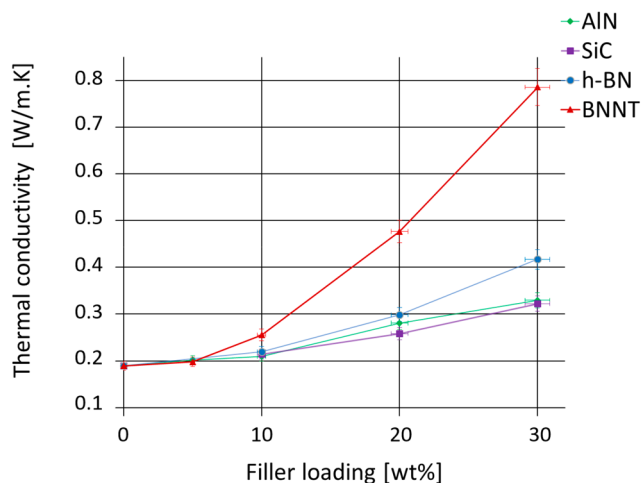


Figure 1. Thermal conductivity values as a function of the loadings in a PCL matrix for four different nanofillers: AlN (green), SiC (purple), h-BN (blue), and BNNTs (red).

below 5 wt % do not lead to significant improvement of the performance whatever the chemical nature of the nanoparticles. A more visible effect appears at higher contents, typically around 10 wt % (which corresponds to about 5% as a volumetric content). Among the nanomaterials without any specific form factor, the most efficient one was h-BN nanofillers. The thermal conductivity was more than doubled (+120% increase) at 30 wt % content, whereas enhancements of 74% and 70% were measured for AlN and SiC nanofillers, respectively, with a similar ratio. This prompted us to look at other existing nanoparticles made of h-BN. Nanotubes of h-BN (BNNTs) have recently emerged as nano-objects of a fast

rising interest.^{24–26} This one-dimensional nanospecies appears as a promising candidate for several reasons. First, its chemical nature is hexagonal boron nitride, known for the combination of high thermal conductivity and electrical insulation properties coming from the large band gap, which is radius and helicity independent.²⁷ Second, the large form factor, defined as the length over diameter ratio, is particularly interesting in our targeted application. Indeed, according to stick percolation theory, such materials are very prone to create a percolative 3D network within matrixes.^{28,29} We thus resumed the study by using BNNTs as a nanofiller.

3.3. BNNT-Based Nanocomposites. Matrixes made of PCL and BNNTs as nanofillers were prepared according to the same protocol, and different loadings were realized. The composites were named PCL–BNNTXX, XX being the weight percentage of the nanofiller (e.g., PCL–BNNT10 is a PCL matrix containing 10 wt % of BNNTs). The thermal conductivity as a function of the nanofiller loading is plotted in Figure 1. It clearly highlights a breakthrough compared to previously studied nanomaterials, in particular with the h-BN nanoparticles, which are similar from the chemical nature point of view. The improvement of thermal conductivity is striking, with for instance a gain of 415% compared to pure PCL at 30 wt %, with a measured value of $0.79 \text{ W}\cdot\text{m}^{-1}\cdot\text{K}^{-1}$. Although a 30 wt % loading of BNNTs is consistent with similar studies using Cu nanoparticles,³⁰ graphite flakes,³¹ or ceramic–BNNT nanocomposites,³² it may appear rather high regarding the current price of BNNTs. However, their fabrication cost is expected to decrease shortly regarding both the fast growing demand and the development of cost-efficient processes.³³

Having in hand a promising nanocomposite, we first performed a set of characterizations for a better understanding of the thermal properties. The thermal degradation of the two raw materials (BNNTs and PCL) and a nanocomposite was explored by TGA, and the results are plotted in Figure 2.

No weight loss was measured for pristine BNNTs up to 600 °C, which is in agreement with other reports.^{34,35} Complete degradation of PCL was observed between 520 °C and 530 °C. As expected, the residual mass content at high temperature of PCL–BNNT10 is consistent with the introduced amount of BNNTs, i.e., 10 wt %. Onset temperatures of degradation (T_{onset}), set at 5% weight loss, were measured at 340 °C for both pure PCL and PCL–BNNT10. Two degradation temperature peaks (T_{deg}) were observed for both pure PCL and the nanocomposite. These peaks can be ascribed to a two-step degradation process implying first a statistical rupture of the polyester chains via ester pyrolysis reaction, and second the formation of ϵ -caprolactone (the monomeric species) coming from an unzipping depolymerization process.³⁶ T_{deg1} occurs at 385 °C and 395 °C for PCL and PCL–BNNT10, respectively, whereas T_{deg2} is measured at 515 °C for both materials. The slight increase of thermal stability for the nanocomposite is consistent with other recent studies on BNNT-based composites.^{32,37,38} Complementary data on thermal properties were obtained by DSC experiments (Figure S1). It was found that the integration of BNNTs into the PCL matrix does not alter significantly the transition phases because both glass transition and melting temperatures are very close for pure PCL and PCL–BNNT10 (Table S2). Although fillers may generally have a strong impact on the crystallinity of composites, in this case no significant alteration was measured, likewise the recently reported polyacrylonitrile–BNNT nanocomposites.³⁹ The temperature is also a key element for the

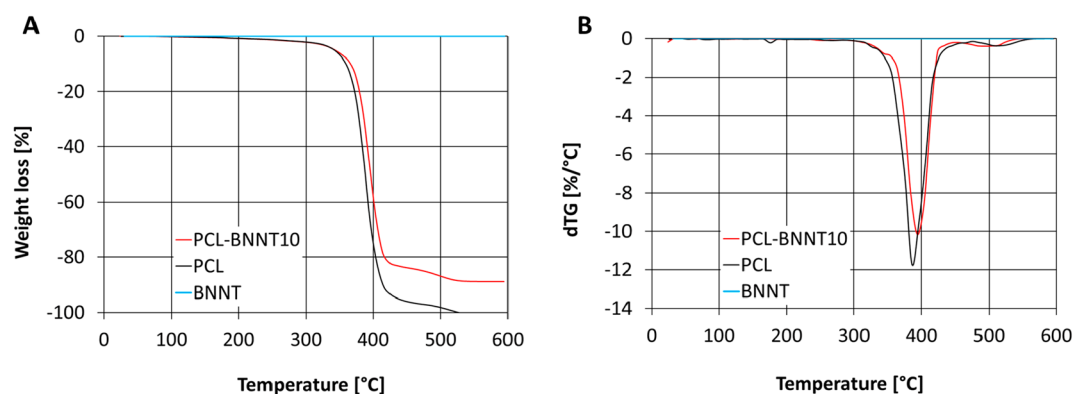


Figure 2. Thermogravimetric analysis in air of pure PCL, BNNTs, and PCL–BNNT10 with (a) weight loss as a function of the temperature and (b) weight loss derivative as a function of the temperature.

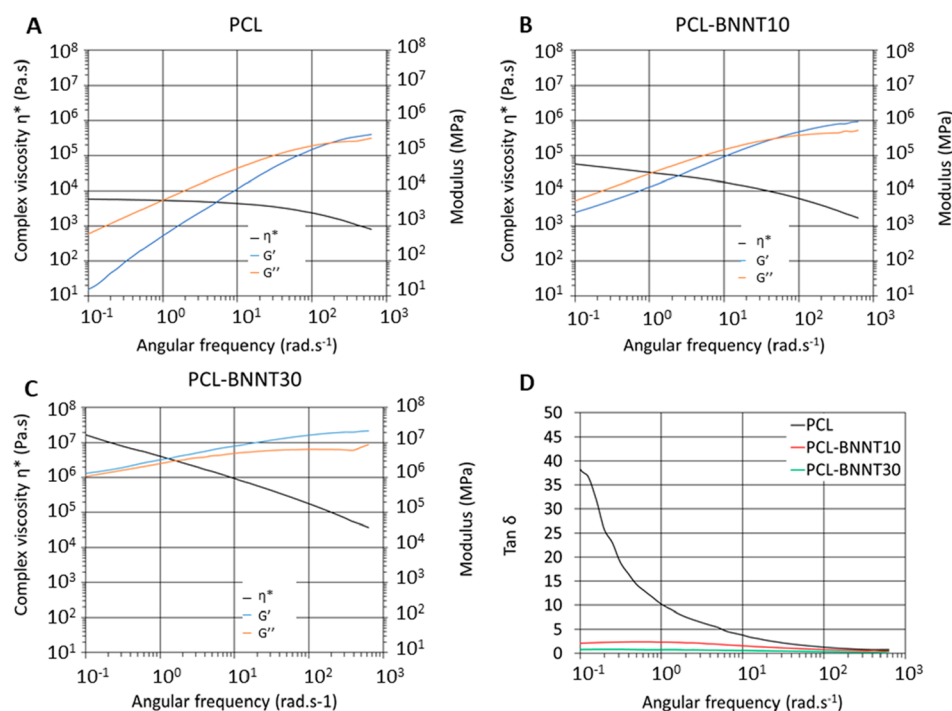


Figure 3. Variation of the complex viscosity (black) and the elastic G' (blue) and loss G'' (orange) moduli at 140 °C and 1% strain for (a) pure PCL, (b) PCL–BNNT10, and (c) PCL–BNNT30. (d) Loss factor ($\tan \delta$) as a function of the angular frequency for pure PCL (black), PCL–BNNT10 (red), and PCL–BNNT30 (green).

nanocomposites' viscosity. Indeed, a potential annoying feature could be the change in viscosity because the flow resistance of the melted filament has to be compatible with the 3D printer system. After performing dynamic amplitude sweep tests to determine the linear viscoelastic region, dynamic frequency sweep experiments were carried out from 1.0×10^{-1} to 6.3×10^2 rad·s⁻¹ with a constant strain rate of 1% in the linear domain at a temperature of 140 °C. The complex viscosity (η^*), elastic modulus (G'), loss modulus (G''), and loss factor ($\tan \delta$) data were recorded against the angular frequency for three materials (BNNTs at 0, 10, and 30 wt % loadings). The results are plotted in Figure 3.

The rheological behavior of pure PCL appears pseudo-plastic, consistently with the literature.⁴⁰ A drastic change for all the above-mentioned parameters is observed upon the introduction of BNNT nanofillers. For instance, the Newtonian region is not observable for the PCL–BNNT30 down to 10^{-1} rad·s⁻¹ which is indicative of a severe alteration of the

rheological properties. This is also clearly noticeable from the loss factor curves presented in Figure 3d. The $\tan \delta$ (loss factor) value describes the ratio of the two portions of the viscoelastic behavior; thus, when $\tan \delta$ is equal to 1, the viscous and elastic behaviors are balanced, and it is the transition point from liquid to solid behavior. At high content (30 wt %), the composite shows a viscoelastic solid behavior in the entire experimental frequency range ($\tan \delta < 1$). The complex viscosity values measured at $\omega = 0.1$ rad·s⁻¹ were 5.89×10^3 , 5.68×10^4 , and 1.71×10^7 Pa·s for PCL, PCL–BNNT10, and PCL–BNNT30, respectively. Thus, the addition of 30 wt % of BNNTs into the PCL matrix leads to an increase of the complex viscosity by a factor 2900 compared to pure PCL, rendering the nanocomposite hardly processable by FFF. A lower viscosity alteration is observed in the presence of 15 wt % of h-BN compared to PCL–BNNT10 (Figure S2). This significant change measured for the BNNT allotrope certainly originates from the dimensionality of the nanoparticles as

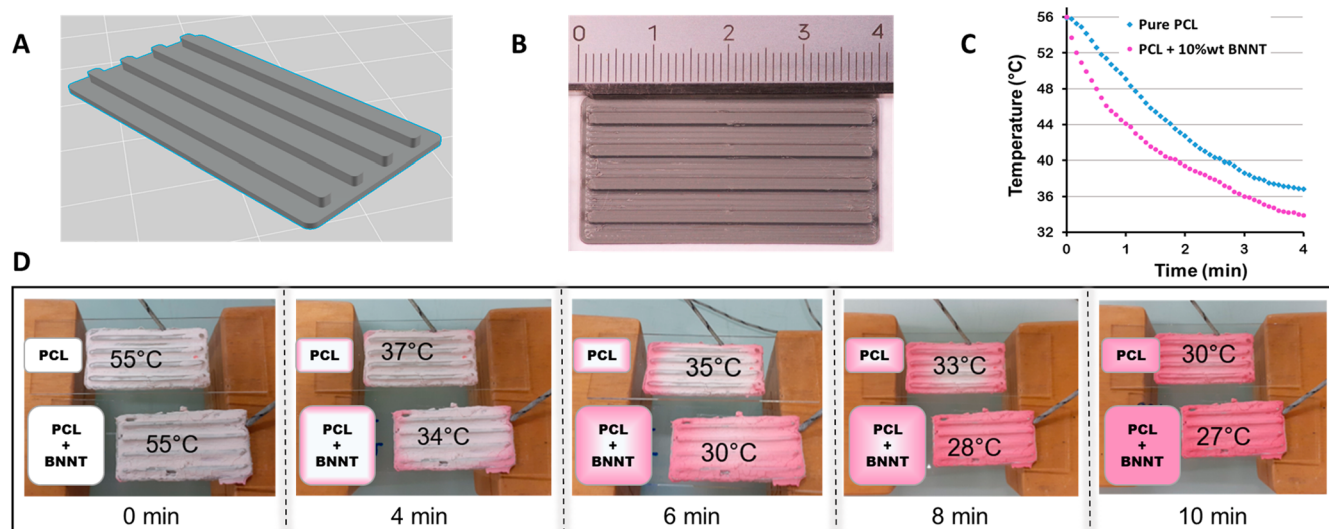


Figure 4. (a) 3D view of the radiator from the STL file. (b) 3D-printed radiator (scale is in centimeters). (c) Temperature as a function of time for the two printed radiators with pure PCL (blue squares) and PCL–BNNT10 nanocomposite (pink circles) filaments. (d) Visual evolution of the cooling of two printed radiators coated with a thermochromic ink.

similarly observed for other nanocomposites,⁴¹ in particular their carbon-based nanomaterials counterparts.⁴² Viscosity alteration in nanocomposites is a well described phenomenon, and loading of fillers is known to often increase dramatically the viscosity, notably for PCL.^{43,44} Though the PCL–BNNT30 nanocomposite holds the best heat dissipation ability, its too high viscosity prevents its use even at high temperature for 3D printing due to flow concerns. We found that the best trade-off for the fabrication of 3D printable filaments was with PCL–BNNT10, having thermal conductivity that is still 35% higher compared to pristine PCL, and the viscosity compatible for most of the additive manufacturing systems.⁴⁵ We ascertained that the electrical performances were not significantly altered: surface conductivity values measured on both pure PCL and PCL–BNNT10 were below the detection threshold of our resistivitymeter, i.e., $10^{-14} \Omega\text{-sq}^{-1}$. As expected, the printable nanocomposite demonstrates good heat dissipation performance associated with a very low electrical conductivity.

Furthermore, a large decrease of the BNNT content within the matrix should be achievable for the fabrication of high performance nanocomposites. Indeed, dispersion of BNNTs is not fully optimized as evidenced by SEM images (Figure S3). Bundles resulting from stabilizing interactions between the BNNTs are formed, which reduces dispersion within the matrix. Although SEM images show the presence of BNNTs within the matrix, it is worth noting that no significant difference is observed between BNNT10 and BNNT30. Unfortunately, SEM images do not provide clear insight into the enhancement of the thermal conductivity (Figure S4). Encouraging results through chemical functionalization of BNNTs have recently been reported, in particular by Simard et al.,^{34,37} and should open the way for greater scattering of the nanofillers in the composite, which should result in an enhanced percolation and thus a higher thermal conductivity at much lower loadings.

3.4. Proof of Concept of Thermal Dissipation Enhancement for 3D Printed Objects. A proof of concept was realized to show that a clear improvement of thermal dissipation could be obtained by the BNNT-based nano-

composites. To obtain a simple and visually perceptible demonstration of the performance, a radiator was produced by 3D-printing. Filaments with a mean diameter of 1.75 mm were fabricated by a common route based on melting of the 10 wt % BNNT nanocomposite, extruding, cooling, and winding onto a spool. Two radiators were then 3D printed, using pure PCL and PCL–BNNT10 filaments. Printing parameters are detailed in Experimental Section, and pictures of the radiators under different angles are provided in Figure S5. They were placed on glass substrates, and K-type thermocouples were used to monitor the temperature. In addition, the printed objects were covered with a thermochromic ink, a chemical product that undergoes a color change at a specific switching temperature (red \leftrightarrow white at 42 ± 2 °C). The radiators were thermalized in an oven at 70 °C and then placed in ambient atmosphere. The temperature was recorded as a function of time, and pictures were taken periodically to visualize the temperature-dependent color change (Figure 4). The temperature of the nanocomposite-based radiator decreased more rapidly, which is indicative of its improved heat dissipation capacity. This proof of concept shows that the use of BNNT nanocomposites can lead to improved performance for FFF-fabricated objects.

4. CONCLUSION

In summary, we report the use of boron nitride nanotubes as promising nanofillers for the fabrication of 3D printable nanocomposites. This one-dimensional nanospecies demonstrates high potential for improving the heat conductivity of nanocomposites while keeping the electrical conductivity at a very low level. We show that the nanofiller content has also a strong impact on the viscosity of the materials, and that a trade-off is to be found for real application in FFF. We report a proof of concept using PCL–BNNT10, showing significant improvement of heat dissipation when BNNT nanocomposites are used for 3D printed radiators with regard to pristine PCL. There is still room for improvement, in particular through dispersion of the nanofillers within the polymeric matrix. Several approaches are currently ongoing and should allow to decrease the content of BNNT by improving the percolative

3D network of nanotubes within the matrix. We think that this approach could expand the materials portfolio for FFF additive manufacturing and give access to printable low-cost electrically insulating nanocomposites for heat dissipation.

■ ASSOCIATED CONTENT

Supporting Information

The Supporting Information is available free of charge at <https://pubs.acs.org/doi/10.1021/acsnm.1c00365>.

Measured values of density and specific heat capacitance for the PCL matrix and the nanomaterials (Table S1). DSC analysis of pure PCL and PCL–BNNT10 nanocomposite (Figure S1) and associated extracted values (Table S2). Variation of the complex viscosity, storage modulus (G'), and loss modulus (G'') at 100 °C and 1% strain for (a) pure PCL, (b) PCL–BNNT10, (c) PCL–hBN15, (d) loss factor ($\tan \delta$) as a function of angular frequency (Figure S2). SEM images of BNNTs, as raw material and in the nanocomposite (Figure S3 and Figure S4). Setup for the measurement of temperature evolution of 3D printed radiators (Figure S5) (PDF)

■ AUTHOR INFORMATION

Corresponding Author

Jean-Pierre Simonato – CEA, LITEN, DTNM, Université Grenoble Alpes, F-38000 Grenoble, France; Department of Chemistry, Duke University, Durham, North Carolina 27708, United States; orcid.org/0000-0002-0217-4237; Email: jean-pierre.simonato@cea.fr

Authors

Thomas Pietri – CEA, LITEN, DTNM, Université Grenoble Alpes, F-38000 Grenoble, France

Benjamin J. Wiley – Department of Chemistry, Duke University, Durham, North Carolina 27708, United States; orcid.org/0000-0002-1314-6223

Complete contact information is available at: <https://pubs.acs.org/doi/10.1021/acsnm.1c00365>

Notes

The authors declare no competing financial interest.

■ ACKNOWLEDGMENTS

The authors acknowledge Huayu Tong (Duke University) for helping in the 3D printing experiments and Xavier Jacolin (CEA) for TGA measurements. This work was supported by the Agence Innovation Défense (ERE grant to Dr. J. P. Simonato).

■ REFERENCES

- (1) Rezvani Ghomi, E.; Khosravi, F.; Neisiany, R. E.; Singh, S.; Ramakrishna, S. Future of Additive Manufacturing in Healthcare. *Curr. Opin. Biomed. Eng.* **2021**, *17*, 100255.
- (2) Pang, Y.; Cao, Y.; Chu, Y.; Liu, M.; Snyder, K.; MacKenzie, D.; Cao, C. Additive Manufacturing of Batteries. *Adv. Funct. Mater.* **2020**, *30* (1), 1906244.
- (3) Wiese, M.; Thiede, S.; Herrmann, C. Rapid Manufacturing of Automotive Polymer Series Parts: A Systematic Review of Processes, Materials and Challenges. *Addit. Manuf.* **2020**, *36*, 101582.
- (4) Mohd Yusuf, S.; Cutler, S.; Gao, N. Review: The Impact of Metal Additive Manufacturing on the Aerospace Industry. *Metals* **2019**, *9* (12), 1286.

(5) Wang, J.-C.; Dommati, H.; Hsieh, S.-J. Review of Additive Manufacturing Methods for High-Performance Ceramic Materials. *Int. J. Adv. Manuf. Technol.* **2019**, *103* (5–8), 2627–2647.

(6) Buchanan, C.; Gardner, L. Metal 3D Printing in Construction: A Review of Methods, Research, Applications, Opportunities and Challenges. *Eng. Struct.* **2019**, *180*, 332–348.

(7) Mechtcherine, V.; Bos, F. P.; Perrot, A.; da Silva, W. R. L.; Nerella, V. N.; Fataei, S.; Wolfs, R. J. M.; Sonebi, M.; Roussel, N. Extrusion-Based Additive Manufacturing with Cement-Based Materials – Production Steps, Processes, and Their Underlying Physics: A Review. *Cem. Concr. Res.* **2020**, *132*, 106037.

(8) Heinrich, M. A.; Liu, W.; Jimenez, A.; Yang, J.; Akpek, A.; Liu, X.; Pi, Q.; Mu, X.; Hu, N.; Schiffelers, R. M.; Prakash, J.; Xie, J.; Zhang, Y. S. 3D Bioprinting: From Benches to Translational Applications. *Small* **2019**, 1805510.

(9) Narupai, B.; Nelson, A. 100th Anniversary of Macromolecular Science Viewpoint: Macromolecular Materials for Additive Manufacturing. *ACS Macro Lett.* **2020**, *9* (5), 627–638.

(10) Valino, A. D.; Dizon, J. R. C.; Espera, A. H.; Chen, Q.; Messman, J.; Advincula, R. C. Advances in 3D Printing of Thermoplastic Polymer Composites and Nanocomposites. *Prog. Polym. Sci.* **2019**, *98*, 101162.

(11) Wu, H.; Fahy, W. P.; Kim, S.; Kim, H.; Zhao, N.; Pilato, L.; Kafi, A.; Bateman, S.; Koo, J. H. Recent Developments in Polymers/Polymer Nanocomposites for Additive Manufacturing. *Prog. Mater. Sci.* **2020**, *111*, 100638.

(12) Flowers, P. F.; Reyes, C.; Ye, S.; Kim, M. J.; Wiley, B. J. 3D Printing Electronic Components and Circuits with Conductive Thermoplastic Filament. *Addit. Manuf.* **2017**, *18*, 156–163.

(13) Cruz, M. A.; Ye, S.; Kim, M. J.; Reyes, C.; Yang, F.; Flowers, P. F.; Wiley, B. J. Multigram Synthesis of Cu-Ag Core-Shell Nanowires Enables the Production of a Highly Conductive Polymer Filament for 3D Printing Electronics. *Part. Part. Syst. Charact.* **2018**, *35* (5), 1700385.

(14) Spinelli, G.; Lamberti, P.; Tucci, V.; Kotsilkova, R.; Ivanov, E.; Menseidov, D.; Naddeo, C.; Romano, V.; Guadagno, L.; Adami, R.; Meisak, D.; Bychanok, D.; Kuzhir, P. Nanocarbon/Poly(Lactic) Acid for 3D Printing: Effect of Fillers Content on Electromagnetic and Thermal Properties. *Materials* **2019**, *12* (15), 2369.

(15) Nguyen, N.; Park, J. G.; Zhang, S.; Liang, R. Recent Advances on 3D Printing Technique for Thermal-Related Applications. *Adv. Eng. Mater.* **2018**, *20* (5), 1700876.

(16) Xu, X.; Chen, J.; Zhou, J.; Li, B. Thermal Conductivity of Polymers and Their Nanocomposites. *Adv. Mater.* **2018**, *30* (17), 1705544.

(17) Wang, Y.-W.; Huang, C.-Y. Thermal Explosion Energy Evaluated by Thermokinetic Analysis for Series- and Parallel-Circuit NMC Lithium Battery Modules. *Process Saf. Environ. Prot.* **2020**, *142*, 295–307.

(18) Sun, Q.; Liu, J.; Peng, Y.; Wang, A.; Wu, Z.; Chen, M. Effective Heat Dissipation of High-Power LEDs through Creation of Three-Dimensional Ceramic Substrate with Kaolin/Graphene Suspension. *J. Alloys Compd.* **2020**, *817*, 152779.

(19) Billah, K. M. M.; Coronel, J. L.; Halbig, M. C.; Wicker, R. B.; Espalin, D. Electrical and Thermal Characterization of 3D Printed Thermoplastic Parts With Embedded Wires for High Current-Carrying Applications. *IEEE Access* **2019**, *7*, 18799–18810.

(20) Nagata, M.; Yamamoto, Y. Synthesis and Characterization of Photocrosslinked Poly(ϵ -Caprolactone)s Showing Shape-Memory Properties. *J. Polym. Sci., Part A: Polym. Chem.* **2009**, *47* (9), 2422–2433.

(21) Bartnikowski, M.; Dargaville, T. R.; Ivanovski, S.; Hutmacher, D. W. Degradation Mechanisms of Polycaprolactone in the Context of Chemistry, Geometry and Environment. *Prog. Polym. Sci.* **2019**, *96*, 1–20.

(22) Huang, J.; Zhu, Y.; Xu, L.; Chen, J.; Jiang, W.; Nie, X. Massive Enhancement in the Thermal Conductivity of Polymer Composites by Trapping Graphene at the Interface of a Polymer Blend. *Compos. Sci. Technol.* **2016**, *129*, 160–165.

- (23) Botlhoko, O. J.; Ramontja, J.; Ray, S. S. Thermally Shocked Graphene Oxide-Containing Biocomposite for Thermal Management Applications. *RSC Adv.* **2017**, *7* (54), 33751–33756.
- (24) Wang, J.; Lee, C. H.; Yap, Y. K. Recent Advancements in Boron Nitride Nanotubes. *Nanoscale* **2010**, *2* (10), 2028.
- (25) Kim, K. S.; Kim, M. J.; Park, C.; Fay, C. C.; Chu, S.-H.; Kingston, C. T.; Simard, B. Scalable Manufacturing of Boron Nitride Nanotubes and Their Assemblies: A Review. *Semicond. Sci. Technol.* **2017**, *32* (1), 013003.
- (26) Shtansky, D. V.; Firestein, K. L.; Golberg, D. V. Fabrication and Application of BN Nanoparticles, Nanosheets and Their Nano-hybrids. *Nanoscale* **2018**, *10* (37), 17477–17493.
- (27) Blase, X.; Rubio, A.; Louie, S. G.; Cohen, M. L. Stability and Band Gap Constancy of Boron Nitride Nanotubes. *Europhys. Lett. EPL* **1994**, *28* (5), 335–340.
- (28) Zhi, C.; Bando, Y.; Terao, T.; Tang, C.; Kuwahara, H.; Golberg, D. Towards Thermoconductive, Electrically Insulating Polymeric Composites with Boron Nitride Nanotubes as Fillers. *Adv. Funct. Mater.* **2009**, *19* (12), 1857–1862.
- (29) Wu, H.; Li, H.; Zhang, W.; Li, F.; Li, B.; Gao, Y.; Zhao, X.; Zhang, L. Percolation of Polydisperse Nanorods in Polymer Nanocomposites: Insights from Molecular Dynamics Simulation. *Compos. Sci. Technol.* **2020**, *196*, 108208.
- (30) Hwang, S.; Reyes, E. I.; Moon, K.; Rumpf, R. C.; Kim, N. S. Thermo-Mechanical Characterization of Metal/Polymer Composite Filaments and Printing Parameter Study for Fused Deposition Modeling in the 3D Printing Process. *J. Electron. Mater.* **2015**, *44* (3), 771–777.
- (31) Jia, Y.; He, H.; Geng, Y.; Huang, B.; Peng, X. High Through-Plane Thermal Conductivity of Polymer Based Product with Vertical Alignment of Graphite Flakes Achieved via 3D Printing. *Compos. Sci. Technol.* **2017**, *145*, 55–61.
- (32) Jia, Y.; Ajayi, T. D.; Morales, J.; Chowdhury, M. A. R.; Sauti, G.; Chu, S.; Park, C.; Xu, C. Thermal Properties of Polymer-derived Ceramic Reinforced with Boron Nitride Nanotubes. *J. Am. Ceram. Soc.* **2019**, *102* (12), 7584–7593.
- (33) Kim, J. H.; Pham, T. V.; Hwang, J. H.; Kim, C. S.; Kim, M. J. Boron Nitride Nanotubes: Synthesis and Applications. *Nano Converg.* **2018**, *5* (1). DOI: 10.1186/s40580-018-0149-y.
- (34) Quiles-Díaz, S.; Martínez-Rubí, Y.; Guan, J.; Kim, K. S.; Couillard, M.; Salavagione, H. J.; Gómez-Fatou, M. A.; Simard, B. Enhanced Thermal Conductivity in Polymer Nanocomposites via Covalent Functionalization of Boron Nitride Nanotubes with Short Polyethylene Chains for Heat-Transfer Applications. *ACS Appl. Nano Mater.* **2019**, *2* (1), 440–451.
- (35) Díez-Pascual, A. M.; Díez-Vicente, A. L. PEGylated Boron Nitride Nanotube-Reinforced Poly(Propylene Fumarate) Nanocomposite Biomaterials. *RSC Adv.* **2016**, *6* (83), 79507–79519.
- (36) Lepoittevin, B.; Devalckenaere, M.; Pantoustier, N.; Alexandre, M.; Kubies, D.; Calberg, C.; Jérôme, R.; Dubois, P. Poly(*ε*-Caprolactone)/Clay Nanocomposites Prepared by Melt Intercalation: Mechanical, Thermal and Rheological Properties. *Polymer* **2002**, *43* (14), 4017–4023.
- (37) Guan, J.; Derdouri, A.; Ashrafi, B.; Benhalima, A.; Kim, K. S.; Daroszewska, M.; Simard, B. Boron Nitride Nanotubes Reinforced Polycarbonate Nanocomposites. *Mater. Today Commun.* **2019**, *20*, 100586.
- (38) Rahman, M. M.; Mateti, S.; Cai, Q.; Sultana, I.; Fan, Y.; Wang, X.; Hou, C.; Chen, Y. High Temperature and High Rate Lithium-Ion Batteries with Boron Nitride Nanotubes Coated Polypropylene Separators. *Energy Storage Mater.* **2019**, *19*, 352–359.
- (39) Chang, H.; Lu, M.; Luo, J.; Park, J. G.; Liang, R.; Park, C.; Kumar, S. Polyacrylonitrile/Boron Nitride Nanotubes Composite Precursor and Carbon Fibers. *Carbon* **2019**, *147*, 419–426.
- (40) Arraiza, A. L.; Sarasua, J. R.; Verdu, J.; Colin, X. Rheological Behavior and Modeling of Thermal Degradation of Poly(*ε*-Caprolactone) and Poly(L-Lactide). *Int. Polym. Process.* **2007**, *22* (5), 389–394.
- (41) Liu, C.; Chen, M.; Zhou, D.; Wu, D.; Yu, W. Effect of Filler Shape on the Thermal Conductivity of Thermal Functional Composites. *J. Nanomater.* **2017**, *2017*, 1–15.
- (42) Kinloch, I. A.; Suhr, J.; Lou, J.; Young, R. J.; Ajayan, P. M. Composites with Carbon Nanotubes and Graphene: An Outlook. *Science* **2018**, *362* (6414), 547–553.
- (43) Bouakaz, B. S.; Habi, A.; Grohens, Y.; Pillin, I. Effect of Combinations of Nanofillers on Rheology-Structure Relations in Biodegradable Poly(*ε*-Caprolactone) Nanocomposites. *Appl. Clay Sci.* **2018**, *161*, 35–47.
- (44) Eriksson, M.; Hamers, J.; Peijs, T.; Goossens, H. The Influence of Graft Length and Density on Dispersion, Crystallisation and Rheology of Poly(*ε*-Caprolactone)/Silica Nanocomposites. *Molecules* **2019**, *24* (11), 2106.
- (45) Gibson, M. A.; Mykulowycz, N. M.; Shim, J.; Fontana, R.; Schmitt, P.; Roberts, A.; Ketkaew, J.; Shao, L.; Chen, W.; Bordeenithikasem, P.; Myerberg, J. S.; Fulop, R.; Verminski, M. D.; Sachs, E. M.; Chiang, Y.-M.; Schuh, C. A.; John Hart, A.; Schroers, J. 3D Printing Metals like Thermoplastics: Fused Filament Fabrication of Metallic Glasses. *Mater. Today* **2018**, *21* (7), 697–702.